recycling

MDPI

Article

Recovery of Valuable Metals from Spent Lithium-Ion Batteries by Combining Reduction Roasting and Selective Leaching

Ruijiao Zhai [1], Kui Huang [1,2,*], Shanjin Mao [1], Rugui Li [1], Haili Dong [1,2] and Xi Zhai [1]

[1] School of Resources, Environment and Materials, Guangxi University, 100 Daxue Road, Nanning 530004, China; 2315303025@st.gxu.edu.cn (R.Z.); 2315393039@st.gxu.edu.cn (S.M.); g62147729@163.com (R.L.); 20120091@gxu.edu.cn (H.D.); 2415303023@st.gxu.edu.cn (X.Z.)

[2] Key Laboratory of Environmental Protection (Guangxi University), Education Department of Guangxi Zhuang Autonomous Region, Nanning 530004, China

* Correspondence: khuang@gxu.edu.cn

Abstract

Amid growing environmental pressure and increasing demand for resource sustainability, the efficient recovery of valuable metals from spent lithium-ion batteries (LIBs) has become a critical challenge in the field of resource recycling. Therefore, a novel approach is presented for selective lithium (Li) and manganese (Mn) separation from $LiNi_xCo_yMn_{1-x-y}O_2$ by combining carbothermic reduction roasting and selective leaching. Low-cost glucose ($C_6H_{12}O_6$) was selected as the reduction roasting reductant, which converts the cathode materials into water-soluble lithium carbonate (Li_2CO_3), water-insoluble cobalt (Co), nickel (Ni), and manganese oxide (MnO). Wet magnetic separation was employed to preferentially extract Li while simultaneously removing excess carbon from Ni, Co, and MnO. Under optimal roasting conditions at 600 °C for 90 min followed by wet magnetic separation with a liquid–solid ratio of 30 mL/g for 30 min, 95.42% of Li was preferentially extracted. Subsequently, at a formic acid (HCOOH) concentration of 1.6 mol/L, liquid–solid ratio of 6 mL/g, and leaching time of 30 min, 94.29% of Mn was selectively extracted from the wet magnetic separation products, whereas Ni and Co were leached at 6.13% and 7.22%, respectively. The acid-leaching residue can be recycled as a Ni-Co alloy.

Keywords: spent lithium-ion batteries; carbothermic reduction roasting; wet magnetic separation; selective leaching; recovery of metals

1. Introduction

In recent years, the global energy structure has rapidly transitioned toward low-carbon energy sources. As a core component of electric vehicles, portable electronic devices, and renewable energy storage systems, LIBs have experienced a substantial increase in demand [1–3]. Ternary LIBs have become the primary power source for electric vehicles owing to their superior energy density, outstanding cycling stability, and elevated operating voltages [4–6]. However, the lifespan of LIBs is typically limited to around 8–10 years [7], after which they are disposed of when their capacity drops to 80% [8,9]. It is anticipated that the scrap volume of ternary LIBs will reach 100 GWh by 2025 [10]. This explosive growth trend poses a severe challenge to recycling technologies [11]. Spent LIBs contain heavy metals and organic volatile compounds that can readily trigger complex chemical reactions upon contact with the environmental media, leading to significant secondary pollution [12,13]. However, ternary LIB cathode materials contain valuable metals such as nickel (Ni), cobalt (Co), manganese (Mn), and lithium (Li), making them important targets

Check for updates

Academic Editor: Silvia Serranti and Dimitrios Kalderis

Received: 3 February 2026
Revised: 25 February 2026
Accepted: 2 March 2026
Published: 10 March 2026

Copyright: © 2026 by the authors. Licensee MDPI, Basel, Switzerland. This article is an open access article distributed under the terms and conditions of the Creative Commons Attribution (CC BY) license.

for resource recovery [14]. With the expansion of the electric vehicle market, the demand for Li, Co, Ni, and Mn is rapidly increasing, causing prices to rise continuously [15,16]. Meanwhile, Li is an important strategic resource. Due to its increasing scarcity and economic significance, it is frequently regarded as a high-value material in the global market [17]. Hence, improper disposal may also result in resource waste and negative economic impacts.

Current mainstream recycling processes for spent LIBs can be divided into three categories: hydrometallurgy, pyrometallurgy, and a combination of both [18,19]. Hydrometallurgy is an efficient and low-energy method for recovering valuable metals [20,21]. However, this method involves a high consumption of chemical reagents and demonstrates limited efficiency in Li recovery [22,23]. Although the pyrometallurgical process is simple to operate, it encounters challenges including incomplete metal recovery and difficulties in achieving effective separation [24,25]. In comparison, the combined process has the advantages of easy operation of pyrometallurgy and high recovery efficiency of hydrometallurgy. In particular, their ability to extract Li preferentially has garnered significant attention [26,27]. Sulfation roasting provides a high extraction efficiency for valuable metals and utilizes cost-effective reductants [28]. Consequently, previous studies have investigated the sulfation roasting process using various sulfiting agents, including sulfuric acid [29], sulfates (such as Na_2SO_4 [30] and $(NH_4)_2SO_4$ [31]), sulfites (such as Na_2SO_3 [32]), and sulfur-containing gases (such as SO_2 [33]). Nevertheless, this method leads to the incorporation of impure elements and release of toxic gases. To develop a green recycling and low-pollution roasting process, C [34], CH_4 [35], and H_2 [36] were used to reduce Ni, Co, and Mn in LIB cathode materials. A reduction roasting process was employed to decrease the valence states of the valuable metals by converting Co, Ni, and Mn into water-insoluble metallic elements or oxides, whereas Li was transformed into water-soluble lithium carbonate (Li_2CO_3) and lithium hydroxide (LiOH). Subsequently, Li was effectively recovered through carbonation water leaching. Furthermore, the water-leaching residue was subjected to sulfuric acid leaching, achieving extraction efficiencies exceeding 94% for Co, Ni, and Mn. Employing graphite from spent LIB anodes as a carbothermal reductant entails resource wastage, given that it is a nonrenewable resource with high recycling potential. By contrast, glucose ($C_6H_{12}O_6$) is cost-effective and readily available, making it a suitable reductant [37]. It should be noted that relevant studies have indicated the inevitable presence of residual carbon in roasted products after carbothermic reduction roasting. These materials readily adsorb metal ions, thereby inhibiting subsequent selective recovery [38]. Ding et al. [39] successfully removed residual carbon substances from water-leaching residues via magnetic separation while selectively recovering Ni, Co, and Mn. In addition, during the acid-leaching process, Ni, Co, and Mn simultaneously dissolve into the leachate, which not only increases the difficulty of the subsequent separation and recovery of valuable metals but also generates significant amounts of wastewater. Therefore, it is essential to develop a process that combines hydrometallurgy and pyrometallurgy to streamline the separation process in the recycling of spent ternary LIBs.

In this study, carbothermal reduction roasting was performed using $C_6H_{12}O_6$ as the reductant, followed by wet magnetic separation to selectively extract Li and effectively remove the excess carbon powder. Subsequently, formic acid (HCOOH) was selected as the leaching reagent for selective Mn leaching because of its reducing properties and mild acidity. At a temperature of 25 °C, a small amount of formic acid (HCOOH) can be used to efficiently and selectively leach Mn from wet magnetic separation products. The Li-rich solution and the acid leachate were, respectively, subjected to evaporative crystallization to prepare high-purity Li_2CO_3 and manganese formate dihydrate ($Mn(HCOO)_2{\cdot}2H_2O$). Additionally, Ni and Co present in the leaching residue were recovered in the form of Ni-Co alloys. The optimal process parameters for carbothermic reduction and selective

leaching were also investigated along with the phase transformations and mechanisms during the roasting and leaching processes.

2. Results and Discussion

2.1. Thermodynamic Analysis

The standard Gibbs free energies ($\Delta_r G_m{}^\theta$) for the reactions that might occur during carbothermic reduction process were calculated using HSC Chemistry 6.0 software. The results are shown in Figure S1. Although the pyrolysis products of $C_6H_{12}O_6$ are complex, the final product is primarily carbon [37]. Consequently, the reactions involved in the carbothermic reduction were categorized into three primary parts, (a) reactions related to carbon, (b) reactions related to the reduction in high-valence metals, and (c) reactions related to Li_2CO_3, as shown in Equations (1)–(14).

$$4LiNi_xCo_yMn_zO_2\ (s) + C\ (s) \rightarrow 2Li_2O\ (s) + 4xNiO\ (s) + 4yCoO\ (s) + 4zMnO\ (s) + CO_2(g) \quad (1)$$

$$C\ (s) + O_2\ (g) \rightarrow CO_2\ (g) \quad (2)$$

$$2C\ (s) + O_2\ (g) \rightarrow 2CO\ (g) \quad (3)$$

$$C\ (s) + CO_2\ (g) \rightarrow 2CO\ (g) \quad (4)$$

$$2CO\ (s) + O_2\ (g) \rightarrow 2CO_2\ (g) \quad (5)$$

$$NiO\ (s) + CO\ (g) \rightarrow Ni\ (s) + CO_2\ (g) \quad (6)$$

$$2NiO\ (s) + C\ (s) \rightarrow 2Ni\ (s) + CO_2\ (g) \quad (7)$$

$$CoO\ (s) + CO\ (g) \rightarrow Co\ (s) + CO_2\ (g) \quad (8)$$

$$2CoO\ (s) + C\ (s) \rightarrow 2Co\ (s) + CO_2\ (g) \quad (9)$$

$$MnO\ (s) + CO\ (g) \rightarrow Mn\ (s) + CO_2\ (g) \quad (10)$$

$$2MnO\ (s) + C\ (s) \rightarrow 2Mn\ (s) + CO_2\ (g) \quad (11)$$

$$Li_2O\ (s) + CO_2\ (g) \rightarrow Li_2CO_3\ (s) \quad (12)$$

$$Li_2CO_3\ (s) \rightarrow Li_2O\ (s) + CO_2(g) \quad (13)$$

$$Li_2CO_3\ (s) + C\ (s) \rightarrow Li_2O\ (s) + 2CO\ (g) \quad (14)$$

It was found that reactions (2)–(4) could occur spontaneously across the entire temperature range, whereas the $\Delta_r G_m{}^\theta$ for reaction (5) remains negative only at temperatures > 700 °C (Figure S1). CO_2 is predominantly produced at temperatures < 700 °C, whereas CO production becomes more favorable at temperatures > 700 °C. Furthermore, the thermodynamic calculations in Figure S1 show that the $\Delta_r G_m{}^\theta$ for reaction (6) is more negative than that for reaction (7), and the $\Delta_r G_m{}^\theta$ for reaction (8) is more negative than that for reaction (9). Therefore, reactions (6) and (8) have stronger driving forces, leading to the preferential reduction in NiO. Moreover, the $\Delta_r G_m{}^\theta$ for reactions (6)–(9) are all negative at temperatures > 250 °C, indicating that both NiO and CoO can be spontaneously reduced to Ni and Co, respectively. Nevertheless, it is difficult to reduce MnO to Mn since the $\Delta_r G_m{}^\theta$ of reactions (10) and (11) remain positive throughout the entire temperature range. Moreover, the $\Delta_r G_m{}^\theta$ for the conversion of Li_2O to Li_2CO_3 (reaction (12)) is negative, indicating that the reaction is thermodynamically favorable. However, it gradually increases with rising temperature, suggesting that excessively high temperatures are unfavorable for the formation of Li_2CO_3. Moreover, although the crystal lattice of Li_2CO_3 exhibits high thermal stability and is resistant to pyrolysis at high temperatures, the addition of carbon resulted

in a decrease in the decomposition temperature. Reaction (14) can occur spontaneously at approximately 990 °C.

To further investigate the reaction characteristics of carbothermal reduction roasting, the cathode powder materials (S-NCM) and its mixture with $C_6H_{12}O_6$ were characterized by TG-DTA analysis. The results demonstrated the superior thermal stability of S-NCM, which exhibited no significant mass loss even at 1000 °C. As shown in Figure 1, the TG-DTA curve for the mixture could be divided into four regions during the roasting process as the temperature increases from 25 to 1000 °C. Region I (<135 °C) featured an endothermic peak at approximately 80 °C, attributed to the removal of free and bound water from the sample [40]. In region II (135–470 °C), an endothermic peak at 145 °C indicated the ongoing thermal decomposition of $C_6H_{12}O_6$ with concomitant gas release, leading to continuous mass loss of the mixture [41]. In region III $C_6H_{12}O_6$ was almost completely pyrolyzed to carbon, and the corresponding DTA curve showed an exothermic peak around 495 °C, which could be attributed to carbothermic reduction. Subsequently, an exothermic peak at 585 °C is assigned to the further reduction in metal oxides to their metallic state [42]. Moreover, an endothermic peak at approximately 660 °C in region IV corresponds to the melting of Li_2CO_3. The subsequent weight loss of the mixture upon further heating may be attributed to the volatilization of Li_2CO_3 [39].

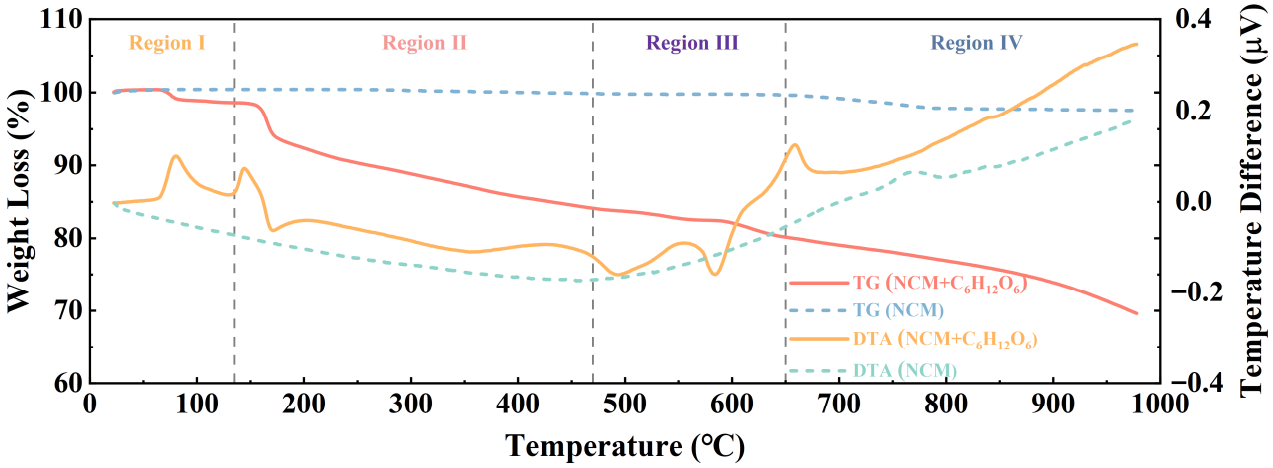


Figure 1. TG-DTA curves of S-NCM and the mixture (80 wt% cathode material and 20 wt% $C_6H_{12}O_6$).

2.2. Preferential Extraction of Lithium by Carbothermic Reduction and Wet Magnetic Separation

2.2.1. Effect of Roasting Temperature

Figure 2a shows the effect of roasting temperature on leaching efficiency of Li. At 450 °C, the efficiency was less than 50%, indicating incomplete destruction of the S-NCM crystal structure. The Li leaching efficiency increased from 48.13% to 95.77% as the roasting temperature was raised from 450 °C to 600 °C, owing to progressively more complete carbothermic reduction. However, further temperature increase led to a decline in efficiency, which is attributed to the phase transformation of Li_2CO_3 under excessive roasting conditions. Excessive roasting causes the melting and subsequent recrystallization of Li_2CO_3, making it more difficult to leach with water. XRD analysis of the roasted products (C-NCM) at different temperatures and the corresponding magnetic separation products (W-NCM) revealed a phase transformation, which accounted for the leaching behavior (Figure 2d). At 450 °C, a small amount of $LiNi_xCo_yMn_{1-x-y}O_2$ remained, demonstrating that S-NCM was partially reduced. With the temperature raised to 500 °C, the diffraction peaks of $LiNi_xCo_yMn_{1-x-y}O_2$ completely disappeared, whereas peaks corresponding to NiO and CoO emerged. At 600 °C, the diffraction peaks of NiO and CoO were replaced by metallic Ni and Co peaks, which intensified at higher temperatures. Concurrently,

the diffraction peaks of Li_2CO_3 initially increased and then gradually diminished with increasing temperature. In addition, the absence of Li_2CO_3 diffraction peaks in the XRD patterns after wet magnetic separation (Figure S2a) indicates the effective separation of Li from Ni, Co, and Mn. Therefore, 600 °C was selected as the optimal roasting temperature for subsequent investigations.

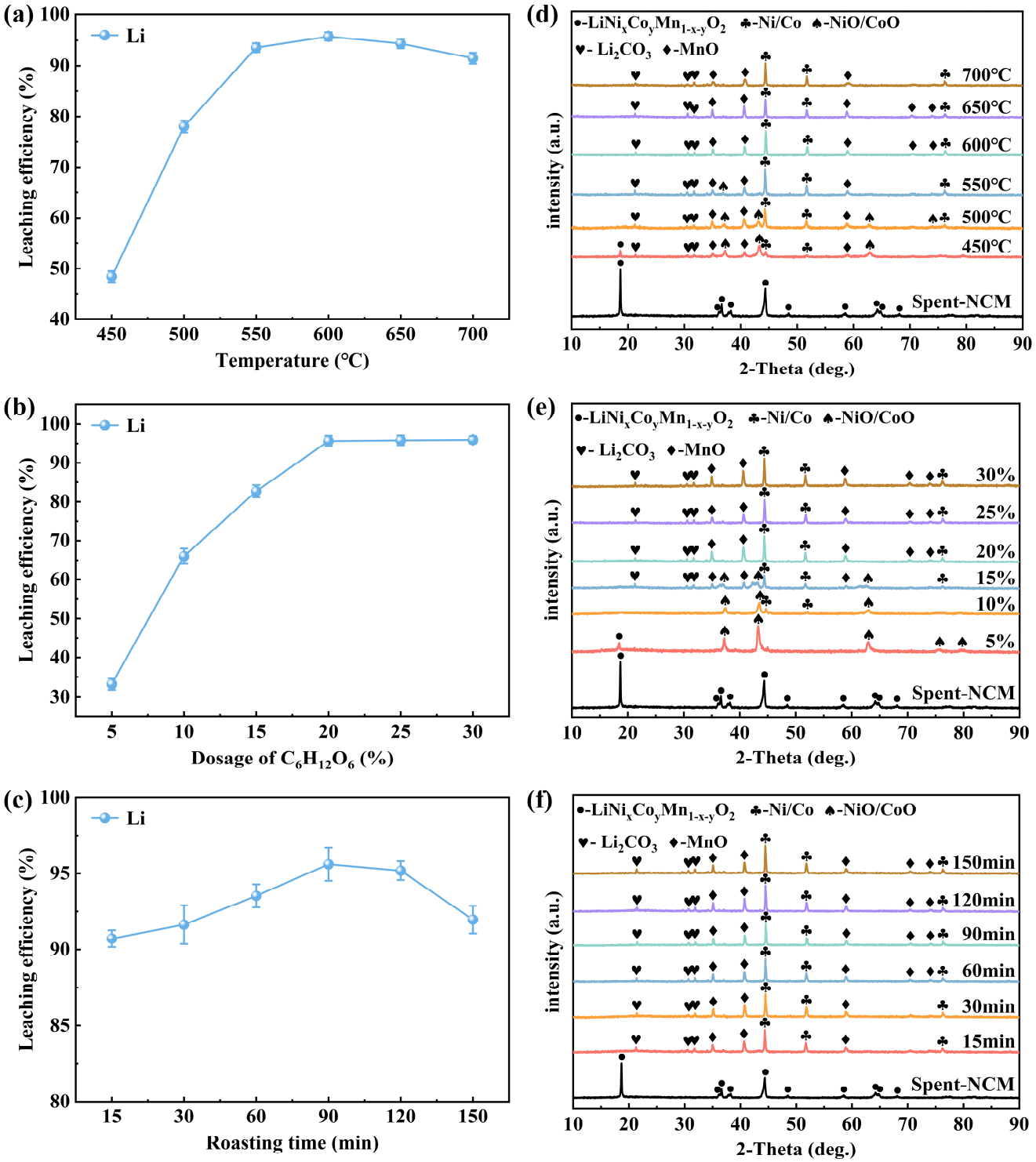


Figure 2. Effects of (**a**) roasting temperature, (**b**) $C_6H_{12}O_6$ dosage, and (**c**) roasting time on Li leaching efficiency; XRD patterns of the roasting products at different (**d**) roasting temperatures, (**e**) $C_6H_{12}O_6$ dosage, and (**f**) roasting time.

2.2.2. Effect of $C_6H_{12}O_6$ Dosage

The effect of $C_6H_{12}O_6$ dosage on the leaching efficiency of Li and the XRD patterns is shown in Figure 2b,e. At the $C_6H_{12}O_6$ dosage of 5%, the Li leaching efficiency was merely 33.25%. Furthermore, XRD patterns of the roasting products still exhibited diffraction peaks corresponding to the $LiNi_xCo_yMn_{1-x-y}O_2$, indicating that 5% $C_6H_{12}O_6$ was insufficient to achieve complete reduction in S-NCM. As the $C_6H_{12}O_6$ dosage increased from 5% to 20%, a gradual increase in Li leaching efficiency was observed. XRD analysis showed that the diffraction peaks of $LiNi_xCo_yMn_{1-x-y}O_2$ completely disappeared and were replaced by peaks corresponding to Ni, Co, and MnO at the 20% $C_6H_{12}O_6$ dosage. The efficiency reached a maximum of 95.61% at the 20% dosage and stabilized thereafter, establishing 20% as the optimal dosage for efficient reduction and Li recovery.

2.2.3. Effect of Roasting Time

Figure 2c illustrates the effect of roasting time on the leaching efficiency of Li at a roasting temperature of 600 °C and a $C_6H_{12}O_6$ dosage of 20%. With the extension of roasting time, the leaching efficiency exhibited an initial increase followed by a subsequent decline. The leaching efficiency of Li reached 95.61% at a roasting time of 90 min. As shown in Figure 2f, the S-NCM crystal structure was destroyed after 15 min of roasting due to the reduction reaction during the heating and cooling processes [43]. As the roasting time increased to 60 and 90 min, the intensities of the diffraction peaks corresponding to Ni and Co gradually increased, indicating that the reduction reaction became increasingly complete. Consequently, the amount of generated Li_2CO_3 increased, enhancing the leaching efficiency of Li. However, when the roasting time reached 120 and 150 min, some Li_2CO_3 formed composite oxides with the low-valence metal oxides, resulting in a decrease in the leaching efficiency of Li [44]. Therefore, 90 min was determined as the optimal roasting time.

2.2.4. Effect of Liquid–Solid Ratio and Leaching Time

The effects of the liquid–solid ratio and leaching time on the selective leaching of Li were systematically investigated under optimal roasting conditions (temperature of 600 °C, $C_6H_{12}O_6$ dosage of 20%, roasting time of 90 min). As shown in Figure 3a, the Li leaching efficiency steadily increased as the liquid–solid ratio rose from 15 to 30 mL/g, reaching a maximum efficiency of 95.42% at 30 mL/g. At a liquid–solid ratio of 15 mL/g, the Li^+ concentration in the leachate reaches 2.43 g/L. Given that the concentration of Li in saturated Li_2CO_3 solution at 25 °C is approximately 2.44 g/L [41], this indicates that the solution approaches saturation, thereby limiting further Li dissolution. However, lower liquid–solid ratios can produce a more concentrated Li-rich leachate, which benefits the subsequent synthesis of Li_2CO_3. When the liquid–solid ratio is 30 mL/g, the Li concentration in the leachate reaches only 1.60 g/L, which is significantly less than that of the saturated solution. Therefore, using a liquid–solid ratio of 30 mL/g is sufficient. According to Figure 3b, when the leaching time increased from 5 to 30 min, the Li leaching efficiency significantly increased to 95.42%. Subsequently, the leaching efficiency of Li leveled off, showing only a marginal increase beyond 30 min, demonstrating that the dissolution of Li was essentially complete after 30 min. Considering these factors comprehensively, a liquid–solid ratio of 30 mL/g and a leaching time of 30 min were selected as the optimal conditions.

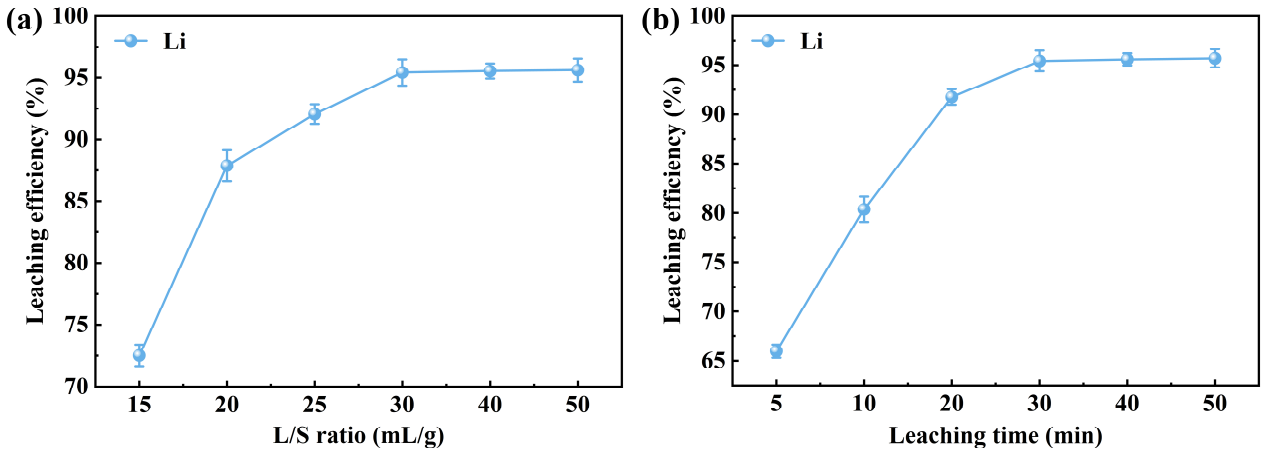


Figure 3. Effects of (**a**) liquid–solid ratio and (**b**) leaching time on Li leaching efficiency from the roasting products (temperature of 600 °C, $C_6H_{12}O_6$ dosage of 20%, and roasting time of 90 min).

2.3. Selective Extraction of Manganese by Acid Leaching

During the selective Li extraction process, water-insoluble Ni, Co, and MnO were not leached, which were almost entirely transformed into wet magnetic separation products. The Ni, Co, and MnO in the products exist as nanocomposite particles after wet magnetic separation, making them resistant to separation by physical methods. Given the different reactivities of metals and metal oxides with acids, HCOOH was employed to selectively leach Mn at 25 °C, thereby achieving separation from Ni and Co. Figure 4a–c shows the effects of HCOOH concentration, leaching time, and the liquid–solid ratio on the leaching efficiencies of Ni, Co, and Mn. Under optimal conditions (HCOOH concentration of 1.6 mol/L, leaching time of 30 min, and liquid–solid ratio of 6 mL/g), the leaching efficiencies of Ni, Co, and Mn were 6.13%, 7.22%, and 94.29%, respectively. Due to differences in leaching behavior, Mn is selectively extracted, while Ni and Co are scarcely leached and remain in the acid-leaching residue (A-NCM).

To investigate the efficacy of reduction roasting combined with wet magnetic separation in enhancing the selective leaching of Mn, samples S-NCM, C-NCM, and W-NCM were leached under identical conditions (HCOOH concentration of 1.6 mol/L, leaching time of 30 min, and liquid–solid ratio of 6 mL/g). In contrast, as shown in Figure 4d, the leaching selectivity for Mn was below 54% when either reduction roasting or wet magnetic separation was omitted from the treatment process.

Table 1 compares the leaching efficiencies of valuable metals from spent lithium batteries using different leaching methods. Notably, Ni, Co, and Mn are hardly leached when only water leaching is applied. Therefore, additional leaching solvents are required to extract Ni, Co, and Mn in the subsequent process. Although H_2SO_4 leaching achieves high leaching efficiencies for Ni, Co, and Mn, it lacks selectivity. In contrast, using HCOOH as the leaching solvent after Li water leaching results in 94.42% Mn leaching, while the leaching efficiencies of Co and Ni are significantly reduced to 7.22% and 6.13%, respectively, demonstrating excellent selectivity. Although $C_6H_8O_7$ can also selectively leach Mn, its selectivity is slightly lower. Among these methods, formic acid stands out due to its high efficiency in leaching Mn and its effective suppression of Co and Ni extraction, making it a viable approach for the selective recovery of metals from spent lithium batteries.

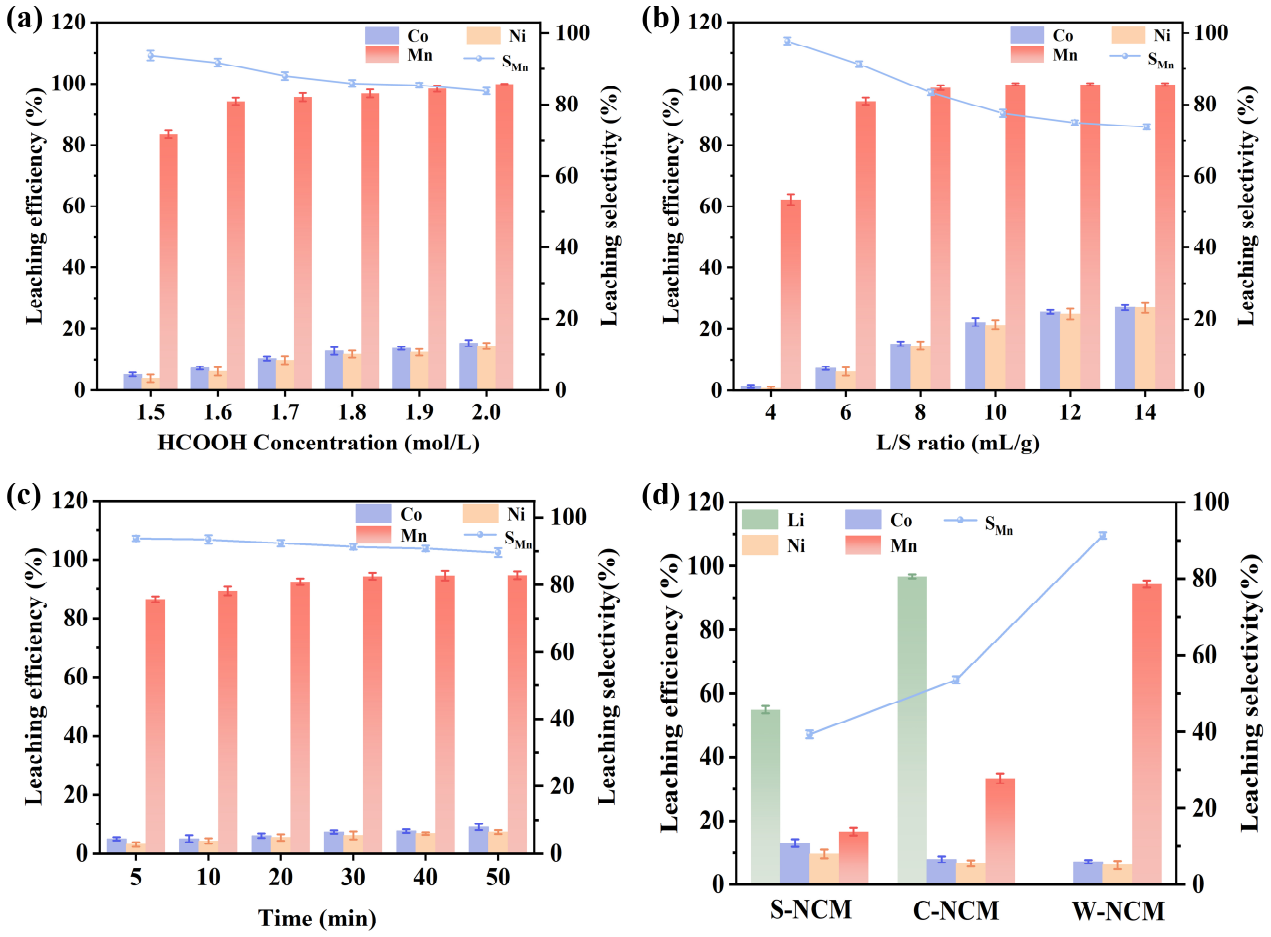


Figure 4. Effects of (**a**) HCOOH concentration, (**b**) liquid–solid ratio, and (**c**) leaching time on Mn leaching selectivity and the leaching efficiencies of Co, Ni, and Mn from W-NCM (temperature of 600 °C, $C_6H_{12}O_6$ dosage of 20%, roasting time of 90 min, liquid–solid ratio of 30 mL/g, and leaching time of 30 min); (**d**) Mn leaching selectivity and the leaching efficiencies of Co, Ni, and Mn from S-NCM, C-NCM, and W-NCM (HCOOH concentration of 1.6 mol/L, leaching time of 30 min, and liquid–solid ratio of 6 mL/g).

Table 1. Comparison of leaching efficiencies of valuable metals from spent lithium-ion batteries using different methods.

Reducing Agent	Leaching Solvent	Li	Ni	Co	Mn	References
$C_6H_{12}O_6$	H_2O, HCOOH	95.42%	6.13%	7.22%	94.29%	This study
Carbon black	H_2O	94.60%		Negligible		[45]
Graphite	H_2O, H_2SO_4	93.33%	94.22%	95.57%	96.63%	[34]
Graphite	H_2O, $C_6H_8O_7$	93.00%	10.00%	14.00%	95.00%	[46]

2.4. Analysis of the Recovery Process

The corresponding phase evolution is detailed in the XRD patterns of S-NCM, C-NCM, W-NCM, and A-NCM powder (Figure 5). After carbothermic reduction roasting, S-NCM was converted to Li_2CO_3, Ni, Co, and MnO. Following wet magnetic separation, the Li_2CO_3 diffraction peak disappeared, while the peaks corresponding to Ni, Co, and MnO remained unchanged, indicating preferential Li extraction. MnO was attracted to the magnetic stirrer along with Co and Ni, which could be attributed to the formation of Ni/MnO nanocomposite particles during the carbothermic reduction process [47]. The MnO particles generated by the reaction wrapped the metallic Ni particles, leading to MnO adsorption by the magnetic stirrer bar. Therefore, the leaching of Li_2CO_3 and separation

of excess carbon powder and magnetic materials can be effectively achieved through wet magnetic separation. Leaching residue XRD pattern analysis after acid leaching revealed the absence of the MnO peak, and only the Ni and Co diffraction peaks remained, indicating that Mn was selectively extracted. This behavior can be explained by the fact that metallic Ni and Co must be oxidized to dissolve, which involves electron transfer from the metals (Ni^0/Co^0 is transferred to Ni^{2+}/Co^{2+}). The weakly acidic and reducing properties of HCOOH provide insufficient H^+ concentration and oxidation capacity to drive this process effectively. MnO is a basic oxide, and its dissolution is an acid–base reaction. This reaction primarily involves protonation of the Mn-O bond by H^+, which facilitates bond cleavage and leads to a comparatively rapid reaction rate. Consequently, leaching with an organic acid characterized by reducing properties and mild acidity at 25 °C can achieve fast and selective Mn extraction while Co and Ni remain predominantly in the residual solids owing to their minimal leaching.

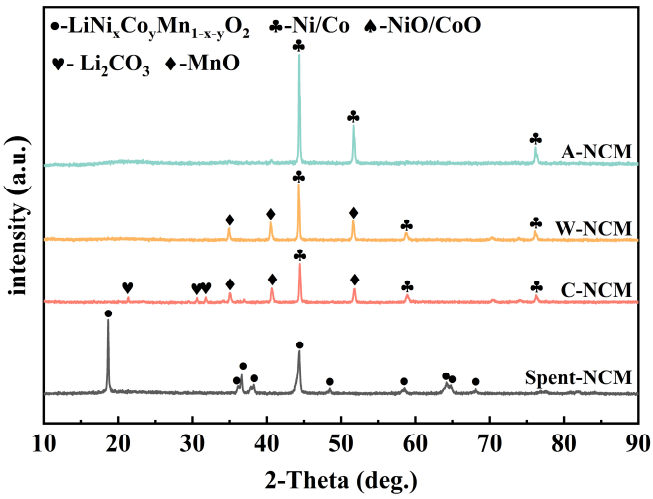


Figure 5. XRD patterns of S-NCM, C-NCM, W-NCM, and A-NCM.

After selective extraction of Mn, the metallic Ni/Co present in the leach residue can be utilized as a Ni-Co alloy in industrial, medical, and materials applications [48]. As shown in the ICP analysis of the leaching residue (Table S1), Li was not detected and Mn was present at a low concentration. The extremely low contents of Li and Mn measured by ICP (below the detection limit of XRD) explain the absence of their corresponding diffraction peaks in the XRD pattern (Figure 5). The purity of the product was approximately 96.13%. The XRD patterns of Li_2CO_3 and $Mn(HCOO)_2{\cdot}2H_2O$ prepared by evaporative crystallization are shown in Figures 6a and 6b, respectively. Their diffraction peaks largely correspond to the standard patterns. The microscopic morphologies of the products are shown in the insets. The corresponding SEM image of the Li_2CO_3 sample appeared as a relatively regular block-like and rod-shaped structure with smooth surfaces, showing well-defined crystallinity in its overall morphology. In contrast, the SEM image of the $Mn(HCOO)_2{\cdot}2H_2O$ sample revealed an irregular block-like structure with a relatively rough surface and evident aggregation. Particle morphologies were diverse, with some particles appearing arranged in stacked formations, demonstrating the typical crystalline characteristics of organic salt materials. The Li_2CO_3 and $Mn(HCOO)_2{\cdot}2H_2O$ contents were determined by ICP analysis, with the results listed in Table S2 and Table S3, respectively. As shown in the tables, Co, Ni, and Mn were not detected in the Li_2CO_3 product. The content of Al was below 0.1%, which is negligible, and the content of other impurities was 0.22%. Therefore, the purity of Li_2CO_3 was calculated to be 99.74%. Regarding $Mn(HCOO)_2{\cdot}2H_2O$, trace amounts of Ni (2.35%), Co (1.02%), and Li (0.36%) were detected. Given their low concentrations,

the corresponding diffraction peaks were not observed in the XRD pattern. The purity of $Mn(HCOO)_2 \cdot 2H_2O$ was consequently 94.28%.

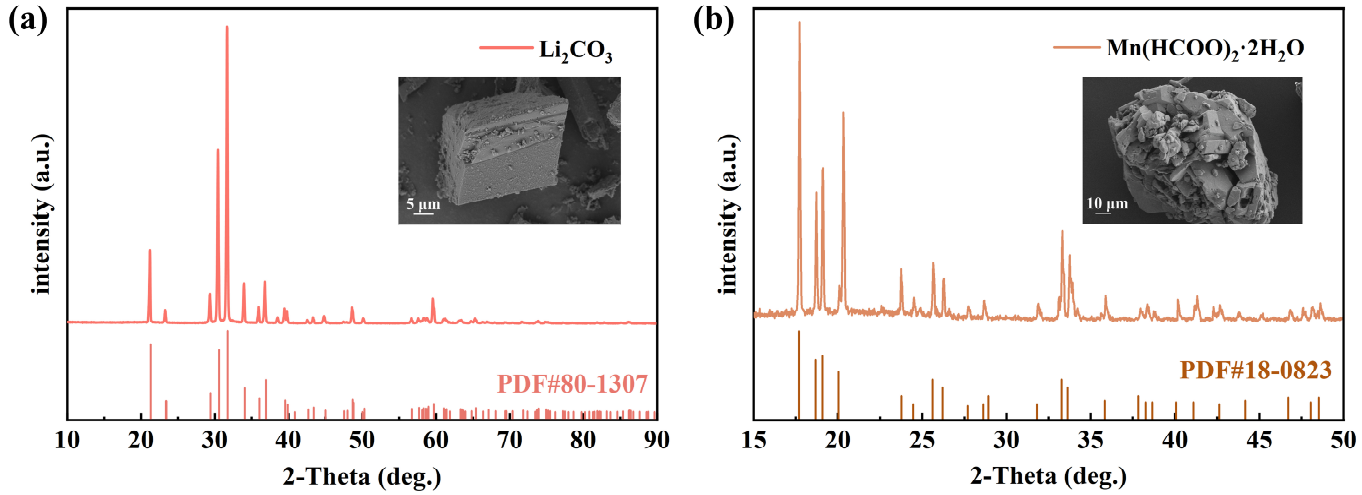


Figure 6. XRD patterns of (**a**) Li_2CO_3 and (**b**) $Mn(HCOO)_2 \cdot 2H_2O$ (The inserted images show the microscopic morphologies of Li_2CO_3 and $Mn(HCOO)_2 \cdot 2H_2O$).

Changes in the valence states of Ni, Co, and Mn were thoroughly investigated using XPS analysis. The Ni 2p XPS profile is presented in Figure 7a. Before carbothermic reduction, two main peaks at 854.99 eV (Ni $2p_{3/2}$) and 872.63 eV (Ni $2p_{1/2}$), along with satellite peaks at 860.40 and 878.75 eV, indicated the presence of Ni^{2+} [49]. After carbothermic reduction roasting, the Ni^{2+} peaks (72.72%) were observed at 856.00, 861.54, 872.46, and 880.02 eV. New fitting peaks observed at 852.92 and 873.75 eV were attributed to metallic Ni (27.28%) [50], demonstrating progressive Ni^{2+} reduction to metallic Ni. Following selective acid leaching for Mn extraction, Ni^{2+} accounted for 75.98% with peaks at 854.69, 860.70, and 878.50 eV. Metallic Ni comprised 24.01%, with a corresponding peak observed at 872.20 eV.

The Co XPS spectrum is shown in Figure 7b. Before carbothermic reduction, the peak at 780.20 eV (Co $2p_{3/2}$) was assigned to Co^{3+} (66.40%), while the peak at 795.21 eV (Co $2p_{3/2}$) corresponded to Co^{2+} (33.60%) [51]. Following carbothermic reduction roasting, Co^{3+} was reduced. Peaks observed at binding energies of 781.10, 787.50, 795.60, 798.42, and 802.43 eV were attributed to Co^{2+} (86.84%), and the peak at 778.20 eV represented metallic Co (13.16%) [26,49]. After selective acid leaching for Mn extraction, the fitting peaks at 777.05 and 797.70 eV were assigned to metallic Co (22.33%). Concurrently, the Co^{2+} peaks at 780.20, 785.40, 795.20, and 802.10 eV still existed; however, their content decreased to 77.67%.

Figure 7c displays the Mn XPS profile. The peaks at 641.96 eV and 653.69 eV corresponded to the Mn $2p_{3/2}$ and Mn $2p_{1/2}$ peaks, respectively, indicating the presence of Mn^{4+} in the cathode materials [52]. After carbothermic reduction roasting, the Mn $2p_{3/2}$ and Mn $2p_{1/2}$ peaks emerged at 641.68 and 653.34 eV, respectively, demonstrating the reduction in Mn^{4+} to Mn^{2+} [53]. Following selective acid leaching for Mn extraction, the Mn^{2+} peaks observed at binding energies of 638.25, 641.50, 646.10, and 652.80 eV remained [50], but their intensities were reduced. This indicated that the content of Mn in the acid-leaching residue was minimal and was effectively extracted. These results collectively demonstrate that carbothermic reduction roasting effectively reduces high-valence metals in the spent LIB powder, which is consistent with the XRD observations. Notably, the valence states of the samples exhibited negligible changes after acid leaching, indicating that the leaching process had no significant effect on the valence states of the metals.

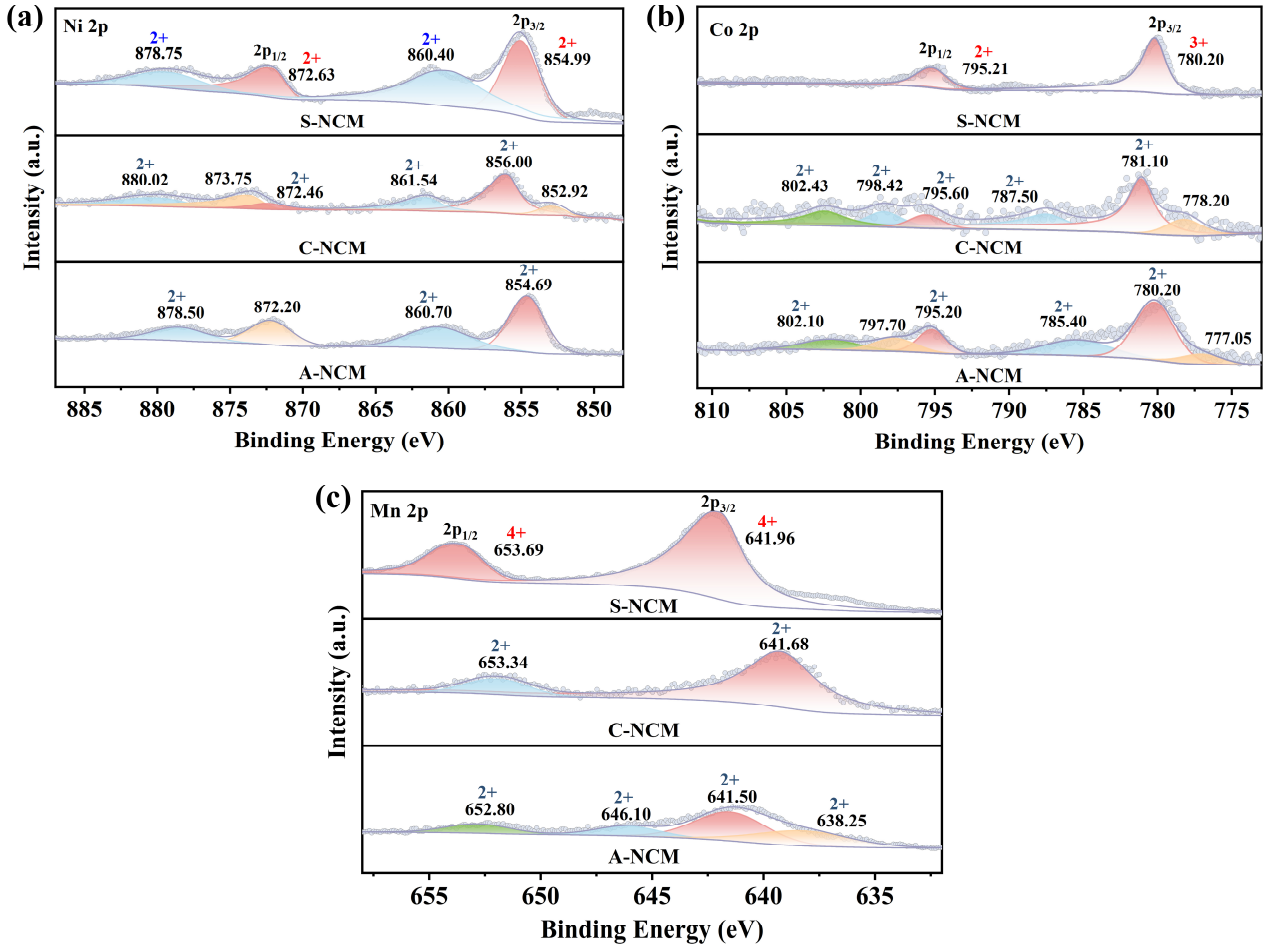


Figure 7. (**a**) XPS spectra of Ni 2p, (**b**) XPS spectra of Co 2p, and (**c**) XPS spectra of Mn 2p.

SEM-EDS was employed to analyze the morphology and elemental distribution of spent LIBs, carbothermic reduction roasted products, wet magnetic separation products, and acid-leaching residue, as illustrated in Figure 8. Figure 8a presents the spent cathode powder prior to roasting, which primarily consists of agglomerated micron-sized spherical or blocky particles. These particles exhibit relatively smooth surfaces and no obvious pores. EDS mapping reveals that the three transition metals (Mn, Co, and Ni) were uniformly distributed throughout the spent cathode powder, with no areas of local enrichment or deficiency.

The SEM image of the roasted products (Figure 8b) reveals an increased degree of particle agglomeration, resulting in larger block-like agglomerates with a dense, rough surfaces and sparse pores. This morphological change was attributed to the interparticle sintering induced by high-temperature calcination, during which the originally dispersed micron-sized particles fused into a dense structure. EDS mapping (Figure 8b) confirms that Mn, Co, and Ni remained uniformly distributed. This indicates that the carbothermal reduction primarily induced phase transformations without altering the spatial arrangement of the metallic elements.

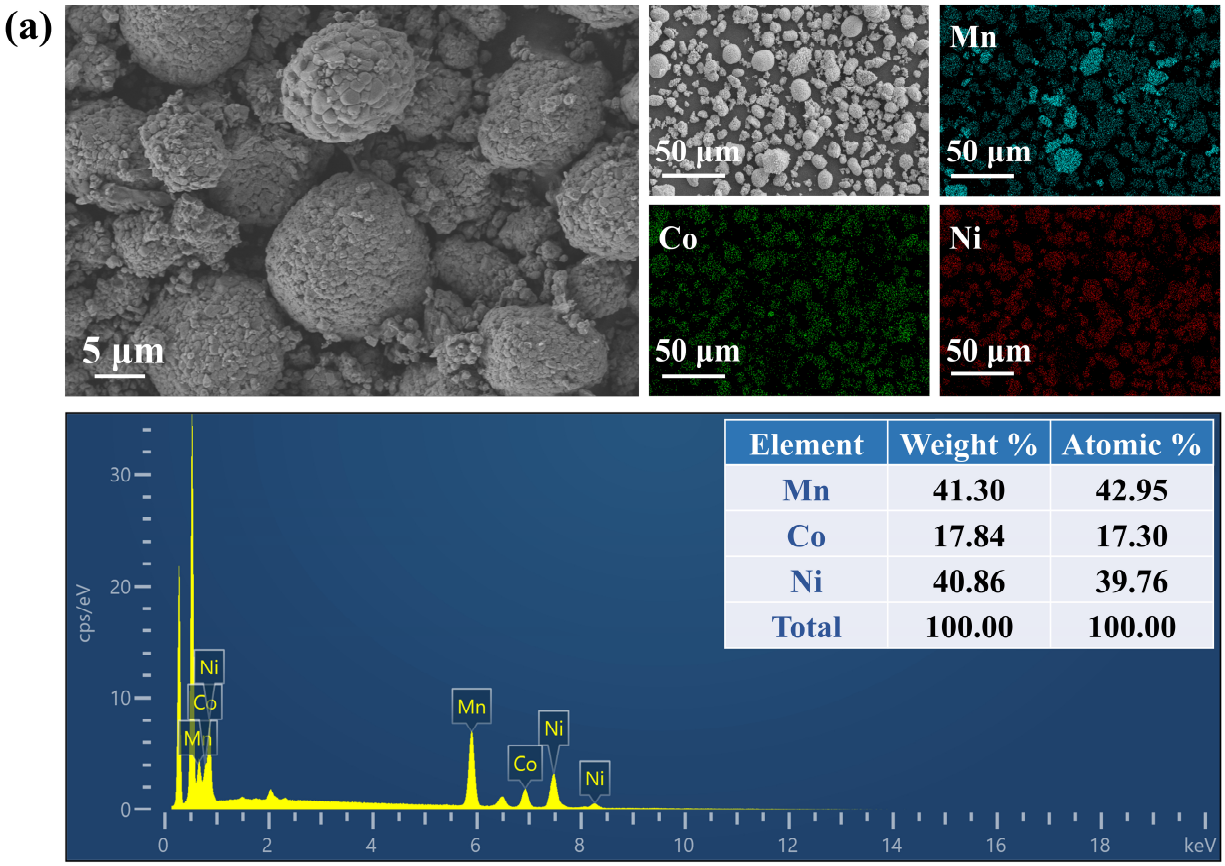
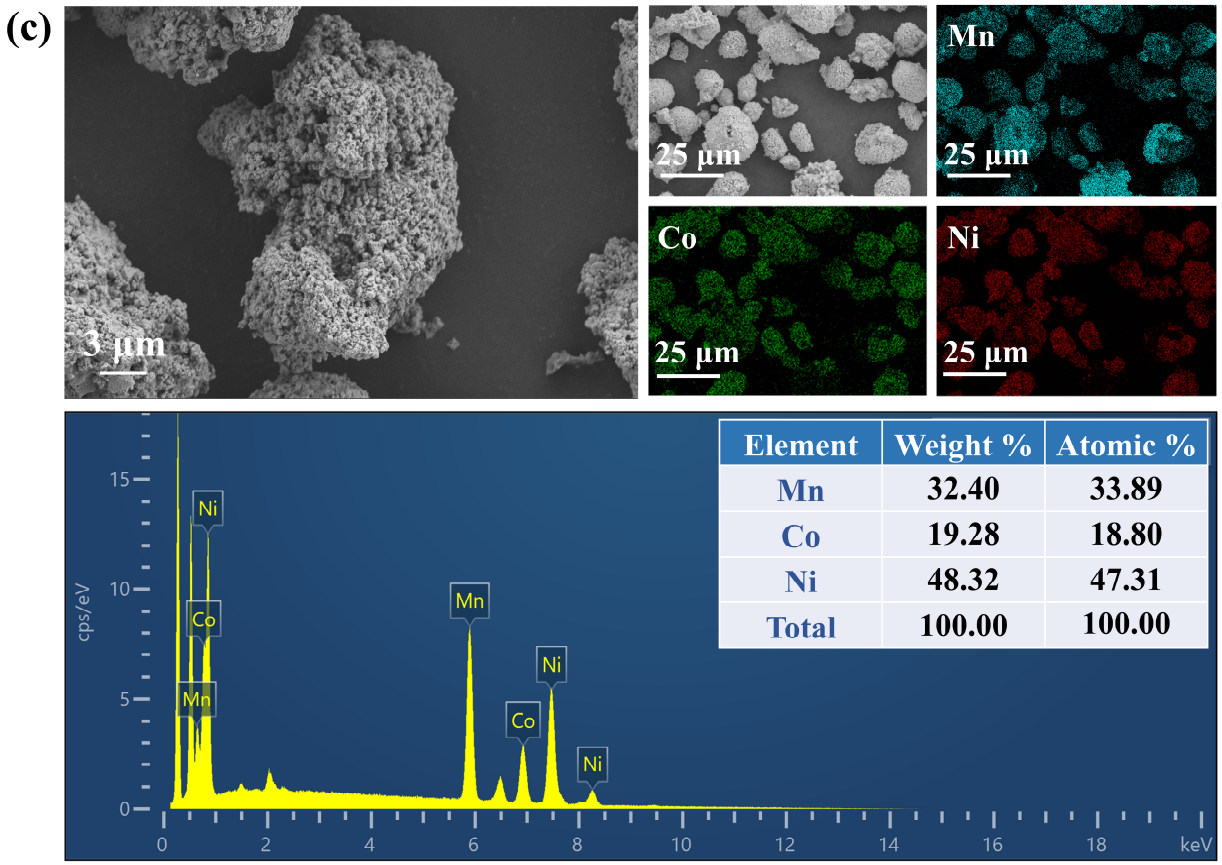


Figure 8. *Cont.*



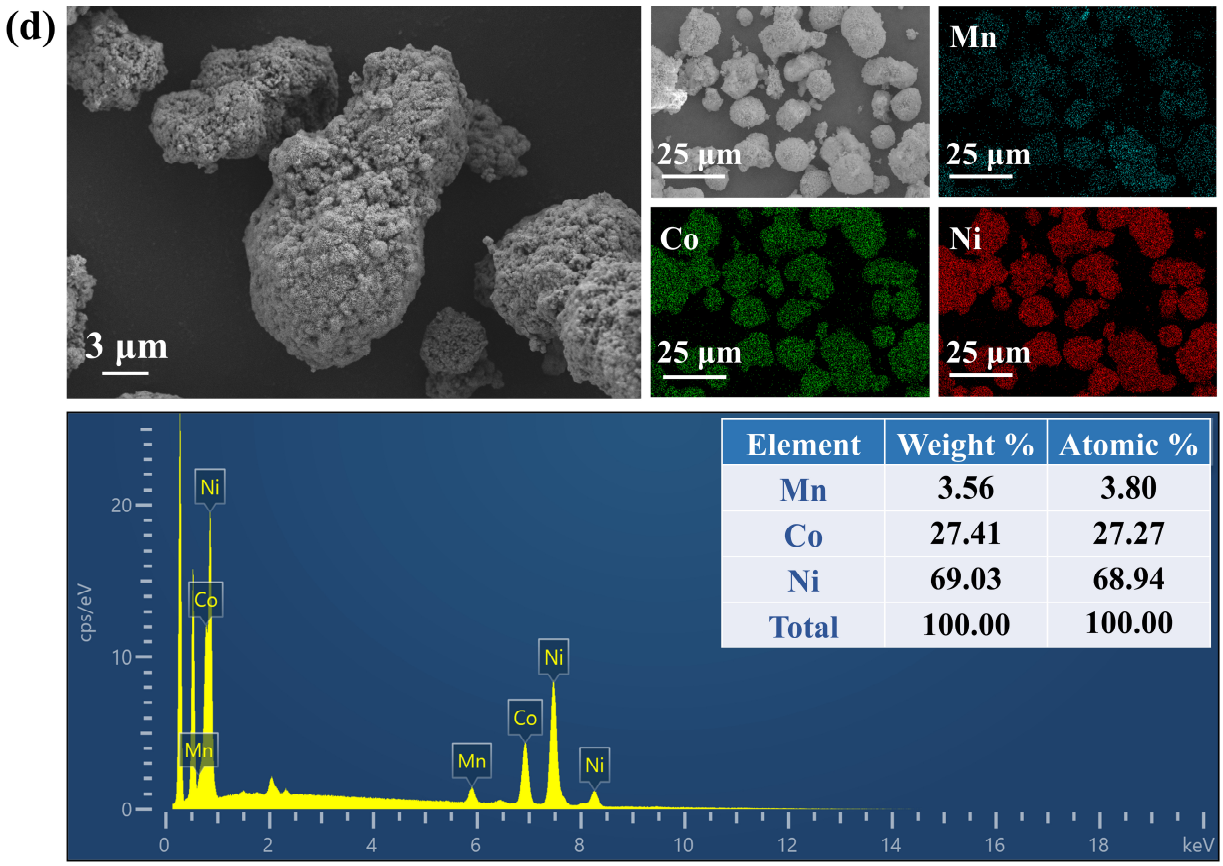


Figure 8. SEM-EDS images of (**a**) spent LIBs, (**b**) carbothermic reduction roasting products, (**c**) wet magnetic separation products, and (**d**) acid-leaching residue.

Figure 8c shows the morphology of the wet magnetic separation products. The material exhibits a porous and loose morphology with nonuniform pore sizes, in contrast to the initial dense structure. This transformation is attributed to the dissolution of soluble Li_2CO_3 during the separation process, wherein the spaces vacated by Li_2CO_3 generate the observed porosity. EDS mapping confirms that Mn, Co, and Ni remained uniformly distributed without localized depletion, demonstrating that wet magnetic separation selectively extracted soluble Li_2CO_3, whereas MnO, Co, and Ni remained undissolved.

Regarding the acid-leaching residue (Figure 8d), the SEM image shows that the number and size of pores in the material further increased. The porous structure loosened, resulting in the formation of smaller fragments. EDS mapping revealed an uneven distribution of Mn, with signals locally weak or absent, in contrast to the relatively uniform distributions of Co and Ni. This indicates that HCOOH selectively dissolves MnO, whereas metallic Co and Ni barely dissolve and remain in the residue. The removal of the crucial framework component MnO creates additional pores at its original sites. This dissolution weakens the structural support, causing some particles to fragment and generate additional fragments.

3. Materials and Methods

3.1. Materials

During this experiment, 18,650 ternary power batteries were recycled from the market. To determine the elemental species and content of the cathode powder, the sample was digested with aqua regia (volume ratio of HCl to HNO_3 = 3:1) in a graphite furnace at 200 °C. After complete dissolution, the solution was analyzed by inductively coupled plasma optical emission spectrometry (ICP-OES) to quantify the elemental composition, and the results are presented in Table 2. The primary reagents used included sodium chloride, hydrochloric acid, nitric acid, hydrogen peroxide, $C_6H_{12}O_6$ and HCOOH, all of which were analytically pure.

Table 2. Elemental composition of spent LIB cathode materials (wt%).

Element	Li	Ni	Co	Mn	Cu	Fe	Al
Content (wt%)	4.86	22.43	9.08	25.25	0.13	0.09	0.42

3.2. Experimental Procedure

The recycling process entails three stages: cathode material pretreatment, selective Li extraction, and selective Mn leaching. First, the spent batteries were discharged, disassembled, and the cathode material was obtained through roasting and screening. Subsequently, Li was selectively extracted via a combined process of carbothermic reduction and wet magnetic separation under optimized conditions, followed by evaporative crystallization of Li_2CO_3 from the leachate. Finally, Mn was leached from the Li-extracted residue using formic acid and recovered as $Mn(HCOO)_2{\cdot}2H_2O$ through evaporative crystallization. The overall process flowsheet for separating and recovering valuable metals from cathode materials is shown in Figure 9.

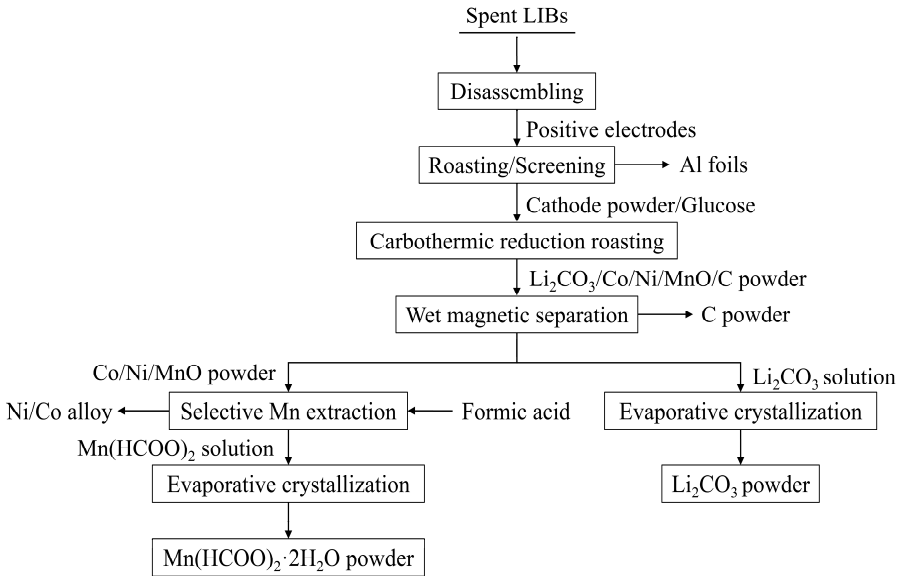


Figure 9. The overall process flowsheet for separating and recovering valuable metals from cathode materials.

3.2.1. Pretreatment

The batteries were immersed in 20% NaCl solution for 48 h to facilitate the discharge process [54,55]. Subsequently, the discharged batteries were manually disassembled to separate the cathodes and anodes. The separated cathodes were then cut into uniformly sized rectangles and placed in a crucible. These samples were subjected to roasting in a muffle furnace at 530 °C for 120 min to remove the binder. Finally, the cathode powder was ground and passed through a 200-mesh sieve to obtain the powder materials for the experiment.

3.2.2. Preferential Li Extraction by Carbothermic Reduction and Wet Magnetic Separation

The cathode powder was mixed with $C_6H_{12}O_6$ in different mass ratios, ground thoroughly, and transferred into a tube furnace. Carbothermic reduction roasting was performed under a nitrogen (N_2) atmosphere at a heating rate of 10 °C/min. The carbothermic reduction products were subjected to wet magnetic separation by adding them to a magnetic stirrer along with an appropriate volume of ultrapure water. Throughout the magnetic separation process, the stirring speed was maintained at 1000 rpm. An Li-rich solution was obtained through water leaching, and the excess carbon powder was removed by filtration. The wet magnetic separation products were collected by isolating the magnetically adsorbed Ni, Co, and Mn. Several parameters affecting the Li leaching efficiency were investigated, including roasting temperature (450–700 °C), roasting time (15–150 min), $C_6H_{12}O_6$ dosage (5–30%), leaching time (5–50 min), and leaching liquid–solid ratio (15–50 mL/g). Li_2CO_3 was produced from the obtained Li-rich solution via evaporation crystallization.

3.2.3. Selective Mn Extraction by Acid Leaching

After selective Li extraction, Mn was leached from the magnetic separation products using HCOOH at a temperature of 25 °C. A certain amount of the W-NCM was placed in a conical flask, and then an HCOOH solution was added. Upon completion of the reaction, the leaching residue and leachate were obtained through solid–liquid separation. The factors affecting the leaching efficiency of Mn were investigated, including HCOOH concentration (5–30%), reaction time (15–150 min), and liquid–solid ratio (5–50 mL/g). The acid leachate was subsequently recovered as $Mn(HCOO)_2 \cdot 2H_2O$ by evaporative crystallization.

3.3. Analytical Method

The leaching efficiencies of the valuable metals and the leaching selectivity of Mn were calculated using Equations (15) and (16), respectively:

$$\eta_i = \frac{C_i \cdot V_i}{m \cdot \omega_i} \times 100\% \quad (15)$$

$$S_{Mn} = \frac{C_{Mn}}{\sum C_i} \times 100\% \quad (16)$$

where η_i (%) and S_{Mn} (%) represent the leaching efficiency of metal element i and the leaching selectivity of Mn, respectively; C_i is the concentration of different metal element i in the leachate (g/L); V_i is the volume of the leachate (L); m is the mass of the cathode material (g); and ω_i is the mass fraction of metal element i in the cathode material (%).

The concentrations of metals in the solution were determined using inductively coupled plasma optical emission spectrometry (ICP-OES, Optima 8000DV, PerkinElmer, Waltham, MA, USA). The composition and crystal structure of the samples were characterized by X-ray powder diffraction (XRD, D8, Bruker AXS GmbH, Karlsruhe, Germany) with Cu-Kα radiation, operating at a scanning speed of 8 °/min. The microstructures and element distributions of the samples were examined using scanning electron microscopy and energy dispersive spectroscopy (SEM-EDS, Gemini SEM 300, Carl Zeiss AG, Oberkochen, Germany). Thermogravimetric analysis (TG-DTA, STA 449 F3, NETZSCH, Selb, Germany) was employed to investigate the reaction properties over the temperature range from 25 to 1000 °C under an argon (Ar) atmosphere with a heating rate of 5 °C/min. The X-ray photoelectron spectroscopy (XPS, K-Alpha, Thermo Fisher Scientific, Waltham, MA, USA) was used to investigate the valence state changes in the elements.

4. Conclusions

In this study, the preferential extraction of Li was achieved through wet magnetic separation following carbothermic reduction roasting, while the separation of Mn from Ni and Co was subsequently accomplished by selective leaching with HCOOH. The proposed methodology facilitates the efficient leaching of Li_2CO_3 and promotes the reduction in Co, Ni, and Mn at lower roasting temperatures, thereby reducing energy consumption and simplifying the subsequent separation and recovery procedures. The TGA results indicate that the addition of $C_6H_{12}O_6$ significantly enhanced the carbothermic reduction reaction. XRD characterization of the carbothermic reduction products revealed that the primary phases formed were metallic Ni, metallic Co, MnO, and Li_2CO_3. The carbothermic reduction roasting combined with wet magnetic separation was optimized to achieve a Li leaching efficiency of 95.42%. Based on the differential reaction rates of metals in different valences with acids, subsequent selective leaching of Mn was performed using HCOOH. Under optimized conditions (1.6 mol/L HCOOH, a liquid–solid ratio of 6 mL/g, and leaching time of 30 min), the leaching efficiency of Mn exceeded 94%, while the leaching efficiencies of Ni and Co were only 6.13% and 7.22%, respectively. The Ni and Co enriched in the acid-leaching residue were recovered as Ni-Co alloys and reintroduced into the production cycle.

The integrated process combining carbothermal reduction, wet magnetic separation, and selective acid leaching achieved the stepwise selective extraction of Li and Mn, as well as the comprehensive recovery of valuable metals. This approach provides an efficient and environmentally friendly recycling strategy with reduced energy consumption and wastewater discharge.

Supplementary Materials: The following supporting information can be downloaded at: https://www.mdpi.com/article/10.3390/recycling11030059/s1, Figure S1: Relationship between $\Delta_r G_m^{\theta}$ and temperature for carbothermic reduction reactions; Figure S2: XRD patterns of the wet magnetic separation products at different (a) roasting temperatures, (b) $C_6H_{12}O_6$ dosage, and (c) roasting time; Table S1: Composition Analysis of the Acid Leach Residue (wt%); Table S2: Composition Analysis of the Li_2CO_3 Products (wt%); Table S3: Composition Analysis of the $Mn(HCOO)_2{\cdot}2H_2O$ Products (wt%).

Author Contributions: Conceptualization, K.H.; methodology, K.H. and H.D.; validation, R.Z.; investigation, R.Z.; data curation, R.Z.; writing—original draft preparation, R.Z.; writing—review and editing, S.M., R.L., H.D. and X.Z.; supervision, K.H.; funding acquisition, K.H. All authors have read and agreed to the published version of the manuscript.

Funding: This research was supported by the National Natural Science Foundation of China (No. 21767003), the Guangxi Scientific and Technology Plan Project (No. Guike AB24010002), the Scientific Research Foundation of Guangxi University (No. XBZ110928), Young Teachers Innovation Cultivation Program (BRP180247) from Guangxi Bossco Environmental Protection Technology Co., Ltd.

Data Availability Statement: The original contributions presented in this study are included in the article and Supplementary Material. Further inquiries can be directed to the corresponding author.

Acknowledgments: During the preparation of this work, the authors used ChatGPT-4 in order to improve language. After using this tool, the authors reviewed and edited the content as needed and take full responsibility for the content of the publication. The authors are grateful to the reviewers who helped us improve the paper with many pertinent comments and suggestions.

Conflicts of Interest: The authors declare that this study received funding from Guangxi Bossco Environmental Protection Technology Co., Ltd. The funder was not involved in the study design, collection, analysis, interpretation of data, the writing of this article, or the decision to submit it for publication.

Abbreviations

S-NCM	The cathode materials of spent lithium-ion batteries obtained after pretreatment.
C-NCM	The products obtained after the carbothermic reduction roasting of the cathode materials.
W-NCM	The products obtained after the wet magnetic separation of the carbothermic reduction products.
A-NCM	The residue obtained after the selective acid leaching of Mn from the wet magnetic separation products.

References

1. Yuan, M.; Liu, H.; Ran, F. Fast-Charging Cathode Materials for Lithium & Sodium Ion Batteries. *Mater. Today* **2023**, *63*, 360–379. [CrossRef]
2. Zhao, L.; Tian, L.; Li, J.; Shi, F.; Chang, Y.; Yan, J.; Zhang, H. Recent Progress in the Recycling of Spent Graphite Anodes: Failure Mechanisms, Repair Techniques, and Prospects. *Energy Storage Mater.* **2024**, *71*, 103640. [CrossRef]
3. Xu, P.; Tan, D.H.S.; Jiao, B.; Gao, H.; Yu, X.; Chen, Z. A Materials Perspective on Direct Recycling of Lithium-Ion Batteries: Principles, Challenges and Opportunities. *Adv. Funct. Mater.* **2023**, *33*, 2213168. [CrossRef]
4. Xie, J.; Lu, Y.-C. A Retrospective on Lithium-Ion Batteries. *Nat. Commun.* **2020**, *11*, 2499. [CrossRef]
5. Gupta, V.; Yu, X.; Gao, H.; Brooks, C.; Li, W.; Chen, Z. Scalable Direct Recycling of Cathode Black Mass from Spent Lithium-Ion Batteries. *Adv. Energy Mater.* **2023**, *13*, 2203093. [CrossRef]
6. Liao, H.; Zhang, S.; Liu, B.; He, X.; Deng, J.; Ding, Y. Valuable Metals Recovery from Spent Ternary Lithium-Ion Battery: A Review. *Int. J. Miner. Metall. Mater.* **2024**, *31*, 2556–2581. [CrossRef]
7. Su, Y.; Fei, Z.; Fan, Y.; Fan, C.; Meng, Q.; Peng, X.; Dong, P. Enhanced Selective Lithium Extraction and Regeneration of Spent $LiNi_{1/3}Co_{1/3}Mn_{1/3}O_2$ through Carbon-Sulfur Composite Roasting. *Sep. Purif. Technol.* **2025**, *365*, 132634. [CrossRef]

8. Lou, P.; Guan, M.; Wu, G.; Wu, J.; Yu, H.; Zhang, W.; Cheng, Q. Recycle Cathode Materials from Spent Lithium-Ion Batteries by an Innovative Method. *Ionics* **2022**, *28*, 2135–2141. [CrossRef]
9. Meng, X.; Hao, J.; Cao, H.; Lin, X.; Ning, P.; Zheng, X.; Chang, J.; Zhang, X.; Wang, B.; Sun, Z. Recycling of $LiNi_{1/3}Co_{1/3}Mn_{1/3}O_2$ Cathode Materials from Spent Lithium-Ion Batteries Using Mechanochemical Activation and Solid-State Sintering. *Waste Manag.* **2019**, *84*, 54–63. [CrossRef]
10. Cun, Z.; Xing, P.; Wang, C.; Li, H.; Ma, S.; Sun, Z.; Wang, Q.; Guan, X. Stepwise Recovery of Critical Metals from Spent NCM Lithium-Ion Battery via Calcium Hydroxide Assisted Pyrolysis and Leaching. *Resour. Conserv. Recycl.* **2024**, *202*, 107390. [CrossRef]
11. Rasoulnia, P.; Chen, Q.; Yang, X.; He, C. Recovery of Valuable Metals from End-of-Life Li-Ion Batteries: Technologies, Progress, and Perspectives. *Resour. Conserv. Recycl.* **2025**, *223*, 108497. [CrossRef]
12. Mrozik, W.; Rajaeifar, M.A.; Heidrich, O.; Christensen, P. Environmental Impacts, Pollution Sources and Pathways of Spent Lithium-Ion Batteries. *Energy Environ. Sci.* **2021**, *14*, 6099–6121. [CrossRef]
13. Wei, D.; Wang, W.; Jiang, L.; Chang, Z.; Anwar, H.; Zhou, H.; Dong, B.; Gao, D.; Lei, H.; Chen, Z.; et al. Preferential Extraction of Lithium from Spent $LiCoO_2$ Cathodes and Regeneration of $LiCoO_2$ Cathodes. *J. Environ. Chem. Eng.* **2023**, *11*, 110890. [CrossRef]
14. Fei, Z.; Su, Y.; Zha, Y.; Zhao, X.; Meng, Q.; Dong, P.; Zhang, Y. Selective Lithium Extraction of Cathode Materials from Spent Lithium-Ion Batteries via Low-Valent Salt Assisted Roasting. *Chem. Eng. J.* **2023**, *464*, 142534. [CrossRef]
15. Yoo, E.; Lee, U.; Kelly, J.C.; Wang, M. Life-Cycle Analysis of Battery Metal Recycling with Lithium Recovery from a Spent Lithium-Ion Battery. *Resour. Conserv. Recycl.* **2023**, *196*, 107040. [CrossRef]
16. Tan, J.; Wang, Q.; Chen, S.; Li, Z.; Sun, J.; Liu, W.; Yang, W.; Xiang, X.; Sun, X.; Duan, X. Recycling-Oriented Cathode Materials Design for Lithium-Ion Batteries: Elegant Structures versus Complicated Compositions. *Energy Storage Mater.* **2021**, *41*, 380–394. [CrossRef]
17. Lee, J.; Lee, J.; Lim, E. Recent Progress and Challenges in Potassium-Ion Battery Anodes: Towards High-Performance Electrodes. *Sci. Technol. Adv. Mat.* **2025**, *26*, 2518746. [CrossRef]
18. Leal, V.M.; Ribeiro, J.S.; Coelho, E.L.D.; Freitas, M.B.J.G. Recycling of Spent Lithium-Ion Batteries as a Sustainable Solution to Obtain Raw Materials for Different Applications. *J. Energy Chem.* **2023**, *79*, 118–134. [CrossRef]
19. Ding, W.; Bao, S.; Zhang, Y.; Xin, C.; Chen, B.; Li, J.; Liu, B.; Xia, Y.; Hou, X.; Xu, K. Sustainable Regeneration of High-Performance Cathode Materials from Spent Lithium-Ion Batteries through Magnetic Separation and Coprecipitation. *J. Clean. Prod.* **2024**, *438*, 140798. [CrossRef]
20. Li, Y.; Lv, W.; Huang, H.; Yan, W.; Li, X.; Ning, P.; Cao, H.; Sun, Z. Recycling of Spent Lithium-Ion Batteries in View of Green Chemistry. *Green Chem.* **2021**, *23*, 6139–6171. [CrossRef]
21. Makuza, B.; Tian, Q.; Guo, X.; Chattopadhyay, K.; Yu, D. Pyrometallurgical Options for Recycling Spent Lithium-Ion Batteries: A Comprehensive Review. *J. Power Sources* **2021**, *491*, 229622. [CrossRef]
22. Lv, W.; Wang, Z.; Cao, H.; Sun, Y.; Zhang, Y.; Sun, Z. A Critical Review and Analysis on the Recycling of Spent Lithium-Ion Batteries. *ACS Sustain. Chem. Eng.* **2018**, *6*, 1504–1521. [CrossRef]
23. Lv, W.; Wang, Z.; Zheng, X.; Cao, H.; He, M.; Zhang, Y.; Yu, H.; Sun, Z. Selective Recovery of Lithium from Spent Lithium-Ion Batteries by Coupling Advanced Oxidation Processes and Chemical Leaching Processes. *ACS Sustain. Chem. Eng.* **2020**, *8*, 5165–5174. [CrossRef]
24. Zhong, Y.; Li, Z.; Zou, J.; Pan, T.; Li, P.; Yu, G.; Wang, X.; Wang, S.; Zhang, J. A Mild and Efficient Closed-Loop Recycling Strategy for Spent Lithium-Ion Battery. *J. Hazard. Mater.* **2024**, *474*, 134794. [CrossRef]
25. Wu, J.; Zheng, M.; Liu, T.; Wang, Y.; Liu, Y.; Nai, J.; Zhang, L.; Zhang, S.; Tao, X. Direct Recovery: A Sustainable Recycling Technology for Spent Lithium-Ion Battery. *Energy Storage Mater.* **2023**, *54*, 120–134. [CrossRef]
26. Hu, Q.; Luo, Z.; Zhou, H.; Cao, Z. High-Efficiency Selective Leaching of Valuable Metals from Spent Lithium-Ion Batteries: Effects of $Na_2S_2O_8$ on the Leaching of Metals. *Waste Manag.* **2023**, *167*, 204–212. [CrossRef]
27. Liu, C.; Ji, H.; Liu, J.; Liu, P.; Zeng, G.; Luo, X.; Guan, Q.; Mi, X.; Li, Y.; Zhang, J.; et al. An Emission-Free Controlled Potassium Pyrosulfate Roasting-Assisted Leaching Process for Selective Lithium Recycling from Spent Li-Ion Batteries. *Waste Manag.* **2022**, *153*, 52–60. [CrossRef]
28. Zhou, A.; Zhang, D.; Liu, Z.; Liu, Z. Comprehensive Recovery of Valuable Metals from Spent $LiCoO_2$ Cathode Material by a Method of NH_4HSO_4 Roasting- $(NH_4)_2S$ Leaching. *Chem. Eng. J.* **2024**, *497*, 154573. [CrossRef]
29. Lin, J.; Li, L.; Fan, E.; Liu, C.; Zhang, X.; Cao, H.; Sun, Z.; Chen, R. Conversion Mechanisms of Selective Extraction of Lithium from Spent Lithium-Ion Batteries by Sulfation Roasting. *ACS Appl. Mater. Interfaces* **2020**, *12*, 18482–18489. [CrossRef]
30. Lei, S.; Ding, H.; Yuan, S.; Wen, G.; Han, C.; Dong, Z.; Wang, W. Prioritized Recovery of Lithium from Spent Lithium-Ion Batteries by Synergistic Roasting with Na_2SO_4: Precise Regulation. *Sep. Purif. Technol.* **2025**, *360*, 131128. [CrossRef]

31. Yang, C.; Zhang, J.; Cao, Z.; Jing, Q.; Chen, Y.; Wang, C. Sustainable and Facile Process for Lithium Recovery from Spent $LiNi_xCo_yMn_zO_2$ Cathode Materials via Selective Sulfation with Ammonium Sulfate. *ACS Sustain. Chem. Eng.* **2020**, *8*, 15732–15739. [CrossRef]
32. Yang, Z.; Zhang, Y.; Yu, H.; Liu, L.; Li, Y.; Hao, T.; Meng, Q.; Dong, P. Sodium Sulfite Roasting for Preferential Lithium Extraction from Cathode Material of Spent Lithium-Ion Batteries. *J. Environ. Chem. Eng.* **2023**, *11*, 110060. [CrossRef]
33. Shi, J.; Peng, C.; Chen, M.; Li, Y.; Eric, H.; Klemettinen, L.; Lundström, M.; Taskinen, P. Sulfation Roasting Mechanism for Spent Lithium-Ion Battery Metal Oxides Under SO_2-O_2-Ar Atmosphere. *JOM* **2019**, *71*, 4473–4482. [CrossRef]
34. Wang, J.; You, X.; She, X.; Xue, Q. Research on the Process of Carbon Thermal Reduction for Recovery and Resynthesis of $LiNi_{0.6}Co_{0.2}Mn_{0.2}O_2$. *J. Mater. Cycles Waste Manag.* **2024**, *26*, 346–359. [CrossRef]
35. Yang, C.; Zhang, J.; Yu, B.; Huang, H.; Chen, Y.; Wang, C. Recovery of Valuable Metals from Spent $LiNi_xCo_yMn_zO_2$ Cathode Material via Phase Transformation and Stepwise Leaching. *Sep. Purif. Technol.* **2021**, *267*, 118609. [CrossRef]
36. Pan, C.; Shen, Y. Pyrometallurgical Recycling of Spent Lithium-Ion Batteries from Conventional Roasting to Synergistic Pyrolysis with Organic Wastes. *J. Energy Chem.* **2023**, *85*, 547–561. [CrossRef]
37. Zhang, B.; Xu, Y.; Makuza, B.; Zhu, F.; Wang, H.; Hong, N.; Long, Z.; Deng, W.; Zou, G.; Hou, H.; et al. Selective Lithium Extraction and Regeneration of $LiCoO_2$ Cathode Materials from the Spent Lithium-Ion Battery. *Chem. Eng. J.* **2023**, *452*, 139258. [CrossRef]
38. Makuza, B.; Yu, D.; Huang, Z.; Tian, Q.; Guo, X. Dry Grinding—Carbonated Ultrasound-Assisted Water Leaching of Carbothermally Reduced Lithium-Ion Battery Black Mass Towards Enhanced Selective Extraction of Lithium and Recovery of High-Value Metals. *Resour. Conserv. Recycl.* **2021**, *174*, 105784. [CrossRef]
39. Ding, W.; Bao, S.; Zhang, Y.; Ren, L.; Xin, C.; Chen, B.; Liu, B.; Xiao, J.; Hou, X. Stepwise Recycling of Valuable Metals from Spent Lithium-Ion Batteries Based on in Situ Thermal Reduction and Ultrasonic-Assisted Water Leaching. *Green Chem.* **2023**, *25*, 6652–6665. [CrossRef]
40. Wang, L.; Jiao, X.; Xie, T.; Bian, H.; Ma, J.; Zhang, Z. Waste Treats Waste: An Efficient Co-Pyrolysis Approach for the Preferential Li Extraction from Spent Lithium-Ion Battery Powder Utilizing Coffee Grounds. *Chem. Eng. J.* **2025**, *520*, 165670. [CrossRef]
41. Zhang, B.; Xu, Y.; Zhu, F.; Huang, J.; Gao, J.; Yang, L.; Song, B.; Deng, W.; Zou, G.; Hou, H.; et al. Selective Lithium Extraction and Recycling of High-Value Metals from Spent $LiNi_xCo_yMn_{1-x-y}O_2$ Cathode Materials. *Ind. Eng. Chem. Res.* **2023**, *62*, 13988–14000. [CrossRef]
42. Liu, H.; Liu, G.; Feng, Y.; Gu, J.; Wang, S.; Tang, Y.; Yuan, H.; Chen, Y. Reaction Behaviors and Mechanisms of In-Situ Carbothermal Reduction in Spent Lithium Batteries. *Sep. Purif. Technol.* **2025**, *362*, 131708. [CrossRef]
43. Hu, Q.; Zhong, H.; Cao, Z. High-Efficiency Leaching of Li and Ni from Spent Lithium-Ion Batteries Based on Sodium Persulfate. *Sep. Purif. Technol.* **2023**, *325*, 124653. [CrossRef]
44. Bang, E.Y.; Mumm, D.R.; Park, H.R.; Song, M.Y. Comparison of Lithium Nickel Cobalt Oxides Synthesized from NiO, Co_3O_4, and $LiOH{\cdot}H_2O$ or Li_2CO_3 by Solid-State Reaction Method. *Ceram. Int.* **2012**, *38*, 5699–5705. [CrossRef]
45. Alcaraz, L.; Rodríguez-Largo, O.; Barquero-Carmona, G.; López, F.A. Recovery of Lithium from Spent NMC Batteries through Water Leaching, Carbothermic Reduction, and Evaporative Crystallization Process. *J. Power Sources* **2024**, *619*, 235215. [CrossRef]
46. Shoaei, A.; Firoozi, S. Recovery of Lithium, Cobalt and Nickel from the Spent NMC Li-Ion Battery by Reduction Roasting, Selective Leaching and Precipitation. *Waste Manag.* **2025**, *200*, 114749. [CrossRef]
47. Huang, K.; Xiong, H.; Dong, H.; Liu, Y.; Lu, Y.; Liu, K.; Wang, J. Carbon thermal reduction of waste ternary cathode materials and wet magnetic separation based on Ni/MnO nanocomposite particles. *Process Saf. Environ. Prot.* **2022**, *165*, 278–285. [CrossRef]
48. Yang, X.; Lu, X.; Zhang, W.; Guo, X.; Ren, J.; Xue, H.; Tang, F. Preparation and application of nano-Ni-Co alloy. *J. Nanopart. Res.* **2023**, *25*, 152. [CrossRef]
49. Lu, J.; Tian, C.; Ren, C.; Omran, M.; Zhang, F.; Gao, L.; Chen, G. Priority Recovering of Lithium from Spent Lithium-Ion Battery Cathode Powder by Pyrolysis Reduction of Bidens Pilosa. *J. Clean. Prod.* **2024**, *439*, 140775. [CrossRef]
50. Tian, C.; Zheng, N.; Liu, B.; Vereš, J.; Omran, M.; Tang, J.; Zhang, F.; Chen, G. Pyrolytic Reduction Roasting of Used Ternary Lithium-Ion Battery Cathode Powder Using Coconut Shell Powder for Selective Recovery of Lithium. *Fuel* **2025**, *386*, 134327. [CrossRef]
51. Ma, Y.; Zhou, X.; Tang, J.; Liu, X.; Gan, H.; Yang, J. One-Step Selective Recovery and Cyclic Utilization of Valuable Metals from Spent Lithium-Ion Batteries via Low-Temperature Chlorination Pyrolysis. *Resour. Conserv. Recycl.* **2021**, *175*, 105840. [CrossRef]
52. Yang, Y.; Yang, H.; Cao, H.; Wang, Z.; Liu, C.; Sun, Y.; Zhao, H.; Zhang, Y.; Sun, Z. Direct Preparation of Efficient Catalyst for Oxygen Evolution Reaction and High-Purity Li_2CO_3 from Spent $LiNi_{0.5}Mn_{0.3}Co_{0.2}O_2$ Batteries. *J. Clean. Prod.* **2019**, *236*, 117576. [CrossRef]
53. Guo, J.; Qu, Y.; Shu, S.; Wang, X.; Yin, H.; Chu, Y. Effects of Preparation Conditions on Mn-Based Activated Carbon Catalysts for Desulfurization. *New J. Chem.* **2015**, *39*, 5997–6015. [CrossRef]

54. Ojanen, S.; Lundström, M.; Santasalo-Aarnio, A.; Serna-Guerrero, R. Challenging the Concept of Electrochemical Discharge Using Salt Solutions for Lithium-Ion Batteries Recycling. *Waste Manag.* **2018**, *76*, 242–249. [CrossRef]
55. Rautela, R.; Yadav, B.R.; Kumar, S. A Review on Technologies for Recovery of Metals from Waste Lithium-Ion Batteries. *J. Power Sources* **2023**, *580*, 233428. [CrossRef]

Disclaimer/Publisher's Note: The statements, opinions and data contained in all publications are solely those of the individual author(s) and contributor(s) and not of MDPI and/or the editor(s). MDPI and/or the editor(s) disclaim responsibility for any injury to people or property resulting from any ideas, methods, instructions or products referred to in the content.